Available online at www.sciencedirect.com
SCIENCE DIRECT
Journal of Power Sources 153 (2006) 18–28
JOURNAL OF POWER SOURCES
www.elsevier.com/locate/jpowsour

Numerical evaluation of a parallel fuel feeding SOFC–PEFC system using seal-less planar SOFC stack

M. Yokoo [a,*], K. Watanabe [a], M. Arakawa [a], Y. Yamazaki [b]

[a] *NTT Energy and Environment Systems Laboratories, NTT Corporation, 3-1, Wakamiya, Morinosato, Atsugi-shi, Kanagawa 243-0198, Japan*
[b] *Department of Innovative and Engineered Materials, Interdisciplinary Graduate School of Science and Engineering, Tokyo Institute of Technology, 4259, Nagatsuta, Midoriku, Yokohama-shi, Kanagawa 226-8502, Japan*

Received 7 February 2005; received in revised form 23 March 2005; accepted 23 March 2005
Available online 6 June 2005

Abstract

We propose a system that combines a seal-less planar solid oxide fuel cell (SOFC) stack and polymer electrolyte fuel cell (PEFC) stack. In the proposed system, fuel for the SOFC (SOFC fuel) and fuel for the PEFC (PEFC fuel) are fed to each stack in parallel. The steam reformer for the PEFC fuel surrounds the seal-less planar SOFC stack. Combustion exhaust heat from the SOFC stack is used for reforming the PEFC fuel. We show that the electrical efficiency in the SOFC–PEFC system is 5% higher than that in a simple SOFC system using only a seal-less planar SOFC stack when the SOFC operation temperature is higher than 973 K.

Keywords: Solid oxide fuel cell; Polymer electrolyte fuel cell; Seal-less stack; Combined system; Steam reforming

1. Introduction

Power generating systems in which a solid oxide fuel cell (SOFC) is used in combination with other generating equipment (SOFC combined systems) provide high electrical efficiency exceeding 50% [1]. Higher electrical efficiency can be achieved in SOFC combined systems than in power generating systems using an SOFC only (simple SOFC system) since high-temperature SOFC exhaust heat (≈1073 K) contributes to the electrical efficiency.

Systems that combine an SOFC with a gas turbine (GT) provide higher electrical efficiency than a simple SOFC system because they use the SOFC exhaust heat for the GT [2,3]. However, the electrical efficiency of the SOFC–GT system decreases when the system output decreases [2,3] since energy conversion efficiency in the GT decreases with decreasing system output.

A system combining an SOFC with a polymer electrolyte fuel cell (PEFC) is also attracting attention [4–6]. We have demonstrated by numerical simulation that the SOFC–PEFC system can provide higher electrical efficiency than simple SOFC systems [6]. The main reason for this is that SOFC exhaust heat is used for the reforming of both the SOFC fuel and the PEFC fuel. Much more SOFC exhaust heat is used effectively in the SOFC–PEFC system. Unlike the electrical efficiency in the SOFC–GT system, which decreases when the system output decreases, that in the SOFC–PEFC system remains almost constant when the system output decreases because the energy conversion efficiency in the fuel cells remains almost constant.

In previous studies, a SOFC and a PEFC were connected by feeding the SOFC exhaust fuel to the PEFC [4–6]. We call this type of SOFC–PEFC system a series SOFC–PEFC system, since both cells were connected by series fuel feeding. A schematic diagram of a series SOFC–PEFC system [6] is shown in Fig. 1. Both the SOFC fuel and PEFC fuel is fed to a steam reformer installed inside the SOFC stack. SOFC exhaust heat is used for the steam reforming of both

* Corresponding author. Tel.: +81 46 240 2572; fax: +81 46 270 2702.
E-mail address: m.yokoo@aecl.ntt.co.jp (M. Yokoo).

0378-7753/$ – see front matter © 2005 Elsevier B.V. All rights reserved.
doi:10.1016/j.jpowsour.2005.03.136

Nomenclature

a	constant (K)
b	constant
C	isopiestic specific heat (J mol K^{-1})
d	distance between edge of circular planar SOFC and heat insulator
E	electromotive force (V)
F	Faraday's constant (C mol^{-1})
h	heat transfer coefficient (W M^{-2} K^{-1})
ΔH	enthalpy change at T_{ENTH} (J mol^{-1})
J	current density (A m^{-2})
K	equilibrium constant
l	thickness (m)
L	energy loss ratio to gross AC output
M	molar flow rate (mol s^{-1})
N	number of SOFC stack units in seal-less planar SOFC stack
Nu	non-dimensional heat transfer coefficient
p	partial pressure (MPa)
Q	amount of heat (W)
r	radial coordinate (m)
r_0	radius of the circular planar SOFC (m)
R	gas constant (J mol K^{-1})
T	temperature (K)
U	utilization rate (%)
V	cell voltage (V)
W	output (W)

Greek letters

ϕ	ohmic voltage drop of SOFC (V)
Γ	contact resistance between circular planar SOFC and interconnector (Ω m^2)
η	electrical efficiency (%)
φ	channel height (m)
λ	heat conductivity (W m^{-1} K^{-1})
ρ	resistivity of solid oxide electrolyte at 1073 K (Ω m)
ζ	dc/ac conversion efficiency

Subscripts

ac	alternating current
AIR	air
AMB	ambient
ANO	anode of SOFC
AUX	auxiliary machine
AVE	average
BLOW	air blower
CATH	cathode of SOFC
CEG	combustion exhaust gas
COM	combustion
dc	direct current
ELE	electrolyte
ENTH	enthalpy
EXC	excess
EXH	exhaust
FUEL	fuel
IN	inlet
INS	heat insulator
MAX	maximum
OTHER	other than air blower
OUT	outlet
OX	oxygen
OXI	oxidation
PE	PEFC
PRE	preheating
RAD	radiation heat
REF	reforming
SHIF	shift reaction
SIMP	simple SO state
SO	SOFC
SR	steam reformer
SRR	steam reforming reaction
VAP	vaporization

fuels. The stack configuration of the SOFC is assumed to be a seal-less tubular type with a depleted fuel plenum, and it is assumed that part of SOFC anode exhaust gas is fed to the PEFC stack [6]. Another part of the exhaust gas is recycled in order to feed steam to the steam reformer. The remaining SOFC anode exhaust gas is burnt with SOFC cathode exhaust gas in the combustion plenum.

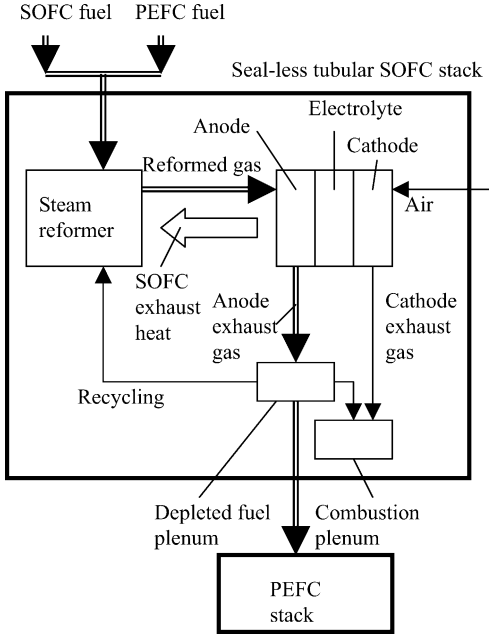

Fig. 1. Schematic diagram of a series SOFC–PEFC system using a seal-less tubular SOFC stack with a depleted fuel plenum.

The seal-less planar SOFC stack without a depleted fuel plenum has been eagerly studied because of its high electrical efficiency of 40% at 1 kW gross dc and simple configuration [7,8]. In such a stack, all of the SOFC anode exhaust gas is burnt with the SOFC cathode exhaust gas around the cells, which makes it impossible to construct a series SOFC–PEFC system. Nonetheless, an SOFC combined system using the seal-less planar SOFC stack is one of the candidates for power sources of the next generation. Here, we propose another type of fuel-feeding SOFC–PEFC system that can use the seal-less planar SOFC stack. We evaluated performance of the system quantitatively by numerical simulation.

Section 2 briefly reviews the configurations of the seal-less planar SOFC stack without depleted fuel plenum and the SOFC–PEFC system that can use it. Sections 3 and 4 describe the simulation models and fundamental equations, respectively. Section 5 discusses the simulation results. Finally, Section 6 summarizes the paper.

2. Configurations

The seal-less planar SOFC stack without a depleted fuel plenum consists of a lot of SOFC stack units as shown in Fig. 2. Each SOFC stack unit consists of a circular planar SOFC and a metallic interconnecter. The circular planar SOFC consists of an anode, electrolyte, and cathode. Fuel and air fed to the center of the circular planar SOFC through a feeding tube are used for power generation as they flow from the center of the circular planar SOFC to its edge. Surrounding the circular planar SOFC is a combustion plenum where unused fuel is burnt with unused oxygen. The steam reformer surrounds the seal-less planar SOFC stack as shown in Fig. 3, so that the stack can be combined with the PEFC stack. PEFC

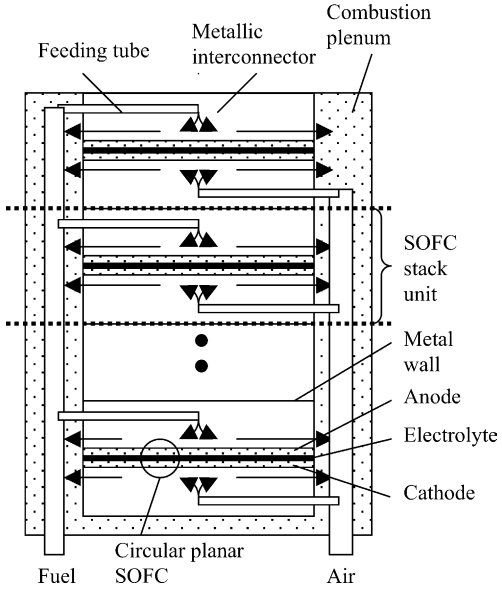

Fig. 2. Seal-less planar SOFC stack without a depleted fuel plenum.

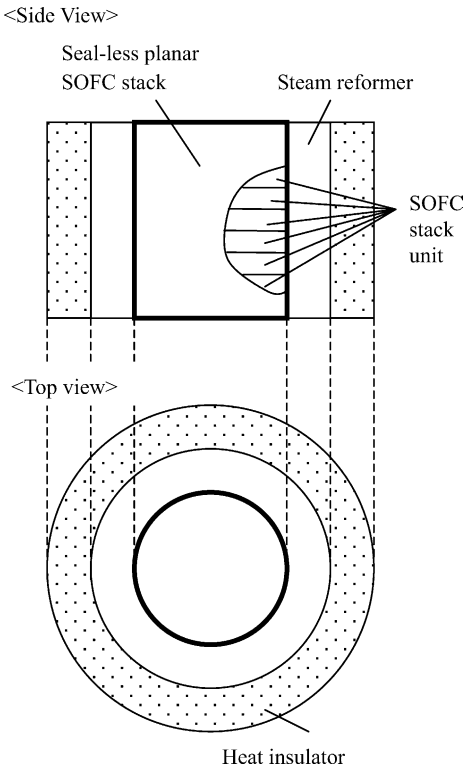

Fig. 3. Seal-less planar SOFC stack without a depleted fuel plenum and steam reformer for PEFC fuel.

fuel is fed to the steam reformer and converted to reformed gas by the steam reforming reaction. The reformed gas produced in the steam reformer is fed to the PEFC stack and used for power generation. Combustion exhaust heat from the seal-less planar SOFC stack is used for the steam reforming reaction. We call this type of SOFC–PEFC system a parallel SOFC–PEFC system, since both fuels are fed to each stack in parallel. A schematic diagram of the parallel SOFC–PEFC system is shown in Fig. 4. Steam for the steam reforming has to be produced by using the combustion exhaust heat in the parallel SOFC–PEFC system since SOFC anode exhaust gas can not be recycled when the seal-less planar SOFC stack has no depleted fuel plenum.

It is reasonable to have the steam reformer surround the seal-less planar SOFC stack since this configuration is similar to that of an actual reformer [9], in which the combustion plenum is inside the steam reforming plenum.

3. Simulation models

3.1. Seal-less planar SOFC stack without depleted fuel plenum

The seal-less planar SOFC stack consists of 41 SOFC stack units. The circular planar SOFC has an electrolyte-supported structure with a radius of 0.06 m. The SOFC stack

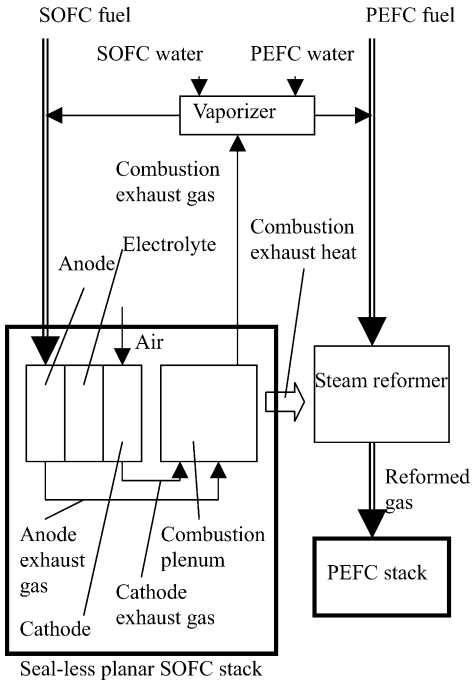

Fig. 4. Schematic diagram of the parallel SOFC–PEFC system using seal-less planar SOFC stack without a depleted fuel plenum.

units are electrically connected to each other through a metallic interconnector and metal wall.

The operation temperature of the circular planar SOFC T_{SO}, which is the maximum temperature in the circular planar SOFC, is the simulation parameter, and it is changed from 873 to 1073 K. The T_{SO} is function of average current density in the circular planar SOFC $J_{SO\text{-}AVE}$ and heat transfer area of heat exchangers.

We made the following assumptions for the simulation of the seal-less planar SOFC stack.

I) The SOFC air and the mixture gas of SOFC methane and steam are distributed to every SOFC stack unit equally and each circular planar SOFC has the same performance.

II) The oxidation of hydrogen,

$$H_2 + \frac{1}{2}O_2 \rightleftarrows H_2O, \quad (1)$$

carbon monoxide,

$$CO + \frac{1}{2}O_2 \rightleftarrows CO_2, \quad (2)$$

and methane,

$$CH_4 + 2O_2 \rightleftarrows 2H_2O + CO_2, \quad (3)$$

occur as cell reactions. The partial pressure of each gas component is in thermodynamic equilibrium at the anode side of circular planar SOFC [10].

III) There is no temperature distribution along with vertical direction in the circular planar SOFC.

IV) The metallic interconnector is madreporite, which has neither electrical nor fluid resistance. And the metal wall has no electric resistance.

V) The feeding tube and flow inside the feeding tube have no influence on the flow and thermal field in the metallic interconnector.

VI) A voltage drop in the circular planar SOFC is caused by ohmic resistance of the electrolyte and contact resistance between the circular planar SOFC and metallic interconnector. Overpotential is included in the ohmic resistance.

VII) Heat is radiated from the steam reformer surrounding the seal-less planar SOFC stack. The heat radiation is proportional to the difference between the SOFC operation temperature T_{SO} and ambient temperature T_{AMB} (298 K)

3.2. Parallel SOFC–PEFC system

The configuration of the parallel SOFC–PEFC system is shown in Fig. 5. Methane (SOFC methane + PEFC methane) is fed to heat exchanger HE1 and preheated. Water (SOFC water + PEFC water) is fed to the vaporizer. The molar ratio of the SOFC methane and water is the same as that of the PEFC methane and water, i.e. 3.0. Steam from the vaporizer is fed to heat exchanger HE2 and preheated. Preheated methane and steam are mixed and a part of the mixture gas is fed to the seal-less planar SOFC stack. The rest of the mixture gas is fed to the steam reformer. The steam reforming reaction of methane,

$$CH_4 + H_2O \rightleftarrows CO + 3H_2, \quad (4)$$

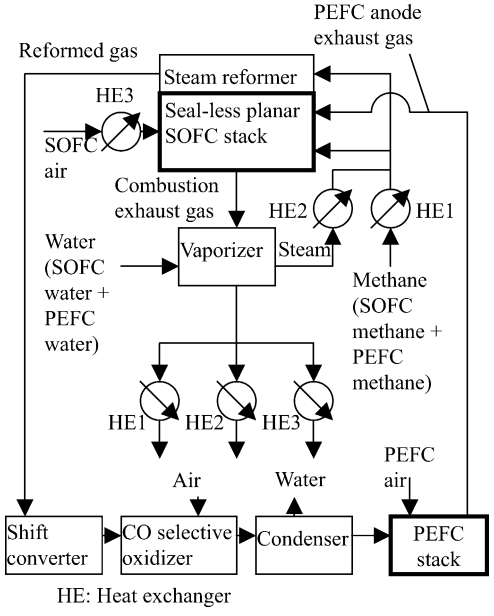

Fig. 5. Parallel SOFC–PEFC system.

and the shift reaction,

$$CO + H_2O \rightleftarrows CO_2 + H_2, \quad (5)$$

occur in the steam reformer. The combustion exhaust heat is used for the steam reforming as mentioned in Section 2. The split ratio of the mixture gas is equal to the molar ratio of the SOFC methane and PEFC methane. SOFC air is fed to the seal-less planar SOFC stack through heat exchanger HE3. Reformed gas is fed to the PEFC stack via the shift converter, CO selective oxidizer, and condenser. The PEFC anode exhaust gas, which contains the hydrogen, is fed to the seal-less planar SOFC stack and burnt in the combustion plenum. Combustion exhaust gas is fed to the vaporizer and combustion exhaust heat is used for vaporizing. Exhaust gas from the vaporizer is divided and fed to HE1–HE3. The gases fed to HE1–HE3 are used for preheating the methane, steam, and air for the SOFC, respectively. Gross dc outputs of both stacks are converted to gross ac outputs by inverters. Net ac output is determined by subtracting the power consumed in an auxiliary machine from the gross ac output.

The heat used for PEFC fuel reforming $Q_{\text{PE-REF}}$ is a simulation parameter and controlled by the air flow rate at the seal-less planar SOFC stack inlet $M_{\text{SO-AIR-IN}}$. In what follows, we will describe the control scheme for $Q_{\text{PE-REF}}$ using Fig. 6. Definitions of terms are as follows:

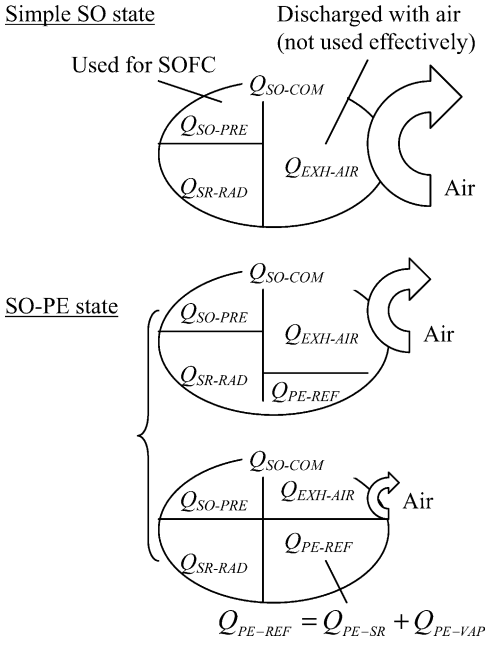

Fig. 6. Schematic diagram of the combustion exhaust heat utilization mechanism.

- Simple SO state: State generating electricity only in the seal-less planar SOFC stack.
- SO-PE state: State generating electricity both in the seal-less planar SOFC and PEFC stacks.
- $Q_{\text{SO-COM}}$: Combustion exhaust heat of the SOFC fuel.
- $Q_{\text{SO-PRE}}$: Part of $Q_{\text{SO-COM}}$ that is used for preheating of SOFC gases and vaporization of SOFC water.
- $Q_{\text{EXH-AIR}}$: Part of $Q_{\text{SO-COM}}$ that is discharged with SOFC air.
- $Q_{\text{SR-RAD}}$: Radiation heat from steam reformer.
- $Q_{\text{PE-VAP}}$: Heat used for vaporization of PEFC water.
- $Q_{\text{PE-SR}}$: Reaction heat used in the steam reformer for the PEFC fuel.
- $Q_{\text{PE-REF}}$: Heat used for PEFC fuel reforming ($Q_{\text{PE-VAP}} + Q_{\text{PE-SR}}$).

Combustion heat $Q_{\text{SO-COM}}$ is expressed as:

$$Q_{\text{SO-COM}} = \begin{cases} Q_{\text{SO-PRE}} + Q_{\text{SR-RAD}} + Q_{\text{EXH-AIR}} & \text{in simple SO state} \\ Q_{\text{SO-PRE}} + Q_{\text{SR-RAD}} + Q_{\text{EXH-AIR}} + Q_{\text{PE-REF}} & \text{in SO-PE state} \end{cases} \quad (6)$$

First, we will show that $Q_{\text{EXH-AIR}} + Q_{\text{PE-REF}}$ is almost totally dominated by the SOFC operation temperature T_{SO}. We assumed that the molar flow rate of SOFC methane at the seal-less planar SOFC stack inlet $M_{\text{SO-CH}_4\text{-IN}}$, the molar flow rate of SOFC water at the seal-less planar SOFC stack inlet $M_{\text{SO-H}_2\text{O-IN}}$, radiation heat $Q_{\text{SR-RAD}}$, and combustion heat $Q_{\text{SO-COM}}$ are only functions of T_{SO}:

$$M_{\text{SO-CH}_4\text{-IN}} = M_{\text{SO-CH}_4\text{-IN}}(T_{\text{SO}}), \quad (7)$$

$$M_{\text{SO-H}_2\text{O-IN}} = M_{\text{SO-H}_2\text{O-IN}}(T_{\text{SO}}), \quad (8)$$

$$Q_{\text{SR-RAD}} = Q_{\text{SR-RAD}}(T_{\text{SO}}), \quad (9)$$

$$Q_{\text{SO-COM}} = Q_{\text{SO-COM}}(T_{\text{SO}}). \quad (10)$$

Since the amount of fuel and water fed to the seal-less planar SOFC stack is a function of T_{SO} [Eq. (7) and (8)], preheating heat $Q_{\text{SO-PRE}}$ is almost completely dominated by T_{SO}:

$$Q_{\text{SO-PRE}} \approx Q_{\text{SO-PRE}}(T_{\text{SO}}). \quad (11)$$

From Eq. (6), (9)–(11), it is clear that $Q_{\text{EXH-AIR}} + Q_{\text{PE-REF}}$ is almost constant for given T_{SO}:

$$Q_{\text{EXH-AIR}} + Q_{\text{PE-REF}} \approx D_1(T_{\text{SO}}), \quad (12)$$

where D_1 is only a function of T_{SO}. Since $Q_{\text{PE-REF}}$ is 0 in the simple SO state, the constant is equal to $Q_{\text{EXH-AIR}}$ in the simple SO state:

$$D_1(T_{\text{SO}}) = Q_{\text{EXH-AIR}}|_{\text{SIMP}}(T_{\text{SO}}). \quad (13)$$

Next, we will show how $Q_{\text{PE-REF}}$ is controlled by air flow rate $M_{\text{SO-AIR-IN}}$. Combustion exhaust heat discharged with air $Q_{\text{EXH-AIR}}$ is almost proportional to air flow rate $M_{\text{SO-AIR-IN}}$:

$$Q_{\text{EXH-AIR}} \approx D_2(T_{\text{SO}}) M_{\text{SO-AIR-IN}}, \quad (14)$$

where D_2 is only a function of T_{SO}. From Eqs. (12)–(14), it is clear that $Q_{\text{PE-REF}}$ is almost solely a function of $M_{\text{SO-AIR-IN}}$

for given T_{SO}:

$$Q_{PE\text{-}REF} \approx D_1(T_{SO}) - Q_{EXH\text{-}AIR} \approx Q_{EXH\text{-}AIR|SIMP}(T_{SO}) - D_2(T_{SO})M_{SO\text{-}AIR\text{-}IN}. \quad (15)$$

Reforming heat $Q_{PE\text{-}REF}$ is increased by decreasing air flow rate $M_{SO\text{-}AIR\text{-}IN}$. The molar flow rate of PEFC methane at the steam reformer inlet $M_{SR\text{-}CH_4\text{-}IN}$ and that of PEFC water at the steam reformer inlet $M_{SR\text{-}H_2O\text{-}IN}$ increase with increasing $Q_{PE\text{-}REF}$.

We made the following assumptions for the simulation of the parallel SOFC–PEFC system:

I) Both the steam reforming reaction of methane and the shift reaction are in thermodynamic equilibrium.
II) The cell reaction in the PEFC stack is the oxidation of hydrogen only [11].
III) The PEFC cell voltage V_{PE}, the PEFC auxiliary power consumption ratio to the net ac output $L_{AUX\text{-}PE}$, and the PEFC fuel utilization ratio $U_{PE\text{-}FUEL}$ are constant and independent of the current density, though V_{SO}, $L_{AUX\text{-}SO}$, and $U_{SO\text{-}FUEL}$ are determined based on the fundamental equations, which will be described in Section 4. The reason for this is that the electrical efficiency at net ac of the actual simple PEFC system using a PEFC stack only, which is proportional to $(1 - L_{AUX\text{-}PE})V_{PE}U_{PE\text{-}FUEL}$, is almost constant [12]. This assumption is reasonable when the PEFC stack is operated within the designed current density region. The simulation shows the performance of the SOFC–PEFC system using a PEFC stack, which is properly designed for the SOFC stack.
IV) Ninety-nine percent of the carbon monoxide in the reformed gas for the PEFC is converted to carbon dioxide according to the shift reaction in the shift converter.
V) Carbon monoxide in the gas fed to the CO selective oxidizer is completely oxidized to carbon dioxide. The reaction in the CO selective oxidizer is the oxidation of carbon monoxide only.
VI) The parallel SOFC–PEFC system cannot be constructed when the temperature of the exhaust gas T_{EXH} is lower than 373 K. This assumption influences the electrical efficiency, but the influence is very small. This is because heat below 373 K can be used only for preheating gases up to 373 K and because the heat needed for preheating gases up to 373 K is very small.

4. Fundamental equations

We use a one-dimensional radial coordinate. The electrical efficiency at the net ac of the parallel SOFC–PEFC system η_{ac} is obtained from Eqs. (16)–(49) as the variable of SOFC operation temperature T_{SO} and the heat used for PEFC fuel reforming $Q_{PE\text{-}REF}$. Constants used in the simulation are listed in Table 1.

Table 1
Constants used in the simulation

Constant	Value	Constant	Value
a	6815 K	Nu_{FUEL}	24
b	−6.35	r_0	6×10^{-2} m
C_{CH_4}	61.9 J mol^{-1} K^{-1}	T_{AMB}	298 K
C_{CO}	31.8 J mol^{-1} K^{-1}	T_{ENTH}	1073 K
C_{CO_2}	50 J mol^{-1} K^{-1}	$U_{PE\text{-}FUEL}$	85%
C_{H_2}	29.9 J mol^{-1} K^{-1}	V_{PE}	0.75 V [18]
C_{H_2O}	44 J mol^{-1} K^{-1}	$\Delta H_{CH_4\text{-}OXI}$	-8.03×10^5 J mol^{-1}
C_{N_2}	31.4 J mol^{-1} K^{-1}	$\Delta H_{CO\text{-}OXI}$	-2.82×10^5 J mol^{-1}
C_{O_2}	33.3 J mol^{-1} K^{-1}	$\Delta H_{H_2\text{-}OXI}$	-2.49×10^5 J mol^{-1}
d	5×10^{-2} m	ΔH_{SHIF}	-3.22×10^4 J mol^{-1}
l_{ANO}	5×10^{-5} m	ΔH_{SR}	2.26×10^5 J mol^{-1}
l_{CATH}	5×10^{-5} m	φ	2×10^{-3} m
l_{ELE}	2×10^{-4} m	Γ	3.5×10^{-5} Ω m^2 [6]
l_{INS}	1×10^{-1} m	$\eta_{SIMP\text{-}dc}$	40%
l_{SO}	1×10^{-2} m	λ_{AIR}	0.073 W m^{-1} K^{-1}
$L_{AUX\text{-}PE}$	0.93	λ_{ANO}	6 W m^{-1} K^{-1}
L_{BLOW}	0.04	λ_{CATH}	11 W m^{-1} K^{-1}
L_{OTHER}	0.03	λ_{ELE}	2.7 W m^{-1} K^{-1}
F	96484 C mol^{-1}	λ_{FUEL}	0.48 W m^{-1} K^{-1}
N	41	ρ	0.167 Ω m
Nu_{AIR}	24	ζ	0.94

4.1. Seal-less planar SOFC stack without a depleted fuel plenum

Equilibrium constants of the oxidation of hydrogen, carbon monoxide, and methane are expressed by:

$$K_{H_2-OXI}(T_{FUEL}(r)) = \frac{p_{H_2O}(r)}{p_{H_2}(r)\sqrt{p_{ANO-O_2}(r)}}, \quad (16)$$

$$K_{CO-OXI}(T_{FUEL}(r)) = \frac{p_{CO_2}(r)}{p_{CO}(r)\sqrt{p_{ANO-O_2}(r)}}, \quad (17)$$

and

$$K_{CH_4-OXI}(T_{FUEL}(r)) = \frac{p^2_{H_2O}(r)p_{CO_2}(r)}{p_{CH_4}(r)p^2_{ANO-O_2}(r)} \quad (18)$$

using the partial pressure of each gas component at the anode side of circular planar SOFC. The mass and energy balance at the anode side of the circular planar SOFC are expressed by:

$$\frac{\partial}{\partial r}[M_{H_2O}(r) + 2M_{CH_4}(r) + M_{H_2}(r)] = 0, \quad (19)$$

$$\frac{\partial}{\partial r}[M_{CO_2}(r) + M_{CH_4}(r) + M_{CO}(r)] = 0, \quad (20)$$

and

$$-\frac{1}{2\pi r}\sum_i C_i \frac{\partial}{\partial r} M_i(r) T_{FUEL}(r) + \frac{T_{ELE}(r)}{2\pi r}\sum_i C_i \frac{\partial}{\partial r} M_i(r) - h_{FUEL}[T_{FUEL}(r) - T_{ELE}(r)] = 0, \quad (21)$$

where i represents methane (CH_4), hydrogen (H_2), steam (H_2O), carbon monoxide (CO), and carbon dioxide (CO_2). The heat transfer coefficient of the flow at the anode side of the circular planar SOFC h_{FUEL} is given by [13]:

$$h_{FUEL} = \frac{\lambda_{FUEL} Nu_{FUEL}}{\varphi}. \quad (22)$$

The mass and energy balances at the cathode side of circular planar SOFC are expressed by:

$$\frac{\partial}{\partial r}\left[2M_{CH_4}(r) + \frac{1}{2}M_{H_2}(r) + \frac{1}{2}M_{CO}(r)\right] = \frac{\partial}{\partial r}M_{CATH\text{-}O_2}(r) \quad (23)$$

and

$$-\frac{1}{2\pi r}\frac{\partial}{\partial r}[M_{CATH\text{-}O_2}(r)C_{O_2}T_{AIR}(r) + M_{N_2}C_{N_2}T_{AIR}(r)] + \frac{C_{O_2}T_{ELE}(r)}{2\pi r}\frac{\partial}{\partial r}M_{CATH\text{-}O_2}(r) - h_{AIR}[T_{AIR}(r) - T_{ELE}(r)] = 0. \quad (24)$$

The heat transfer coefficient of the flow at the cathode side of the circular planar SOFC $h_{SO\text{-}AIR}$ is expressed by:

$$h_{AIR} = \frac{\lambda_{AIR} Nu_{AIR}}{\varphi}. \quad (25)$$

The energy balance in the circular planar SOFC is given by:

$$h_{FUEL}[T_{FUEL}(r) - T_{ELE}(r)] + h_{AIR}[T_{AIR}(r) - T_{ELE}(r)] - \frac{[T_{ELE}(r) - T_{ENTH}]}{2\pi r} \times \left[\sum_i C_i \frac{\partial}{\partial r}M_i(r) + C_{O_2}\frac{\partial}{\partial r}M_{CATH\text{-}O_2}(r)\right] + \frac{\Delta H_{CH_4\text{-}OXI}}{2\pi r}\frac{\partial}{\partial r}M_{CH_4}(r) + \frac{\Delta H_{H_2\text{-}OXI}}{2\pi r}\frac{\partial}{\partial r}M_{H_2}(r) + \frac{\Delta H_{CO\text{-}OXI}}{2\pi r}\frac{\partial}{\partial r}M_{CO}(r) + \frac{(l_{ANO}\lambda_{ANO} + l_{CATH}\lambda_{CATH} + l_{ELE}\lambda_{ELE})}{r} \times \frac{\partial}{\partial r}\left[r\frac{\partial T_{ELE}(r)}{\partial r}\right] = J_{SO}(r)V_{SO}, \quad (26)$$

where the temperature for the definition of enthalpy change T_{ENTH} is 1073 K. The current density of the circular planar SOFC $J_{SO}(r)$ is given [14]:

$$J_{SO}(r) = -\frac{2F}{\pi r}\frac{\partial}{\partial r}M_{CATH\text{-}O_2}(r). \quad (27)$$

The cell voltage of the circular planar SOFC V_{SO} is given by:

$$V_{SO} = E_{SO}(r) - \phi_{SO}(r) - J_{SO}(r)\Gamma, \quad (28)$$

Table 2
Relationship between SOFC operation temperature T_{SO} and average current density in the seal-less planar SOFC stack $J_{SO\text{-}AVE}$

T_{SO} (K)	$J_{SO\text{-}AVE}$ (A m^{-2})
873	1600
923	2100
973	2600
1023	3000
1073	3300

where the electromotive force of the circular planar SOFC $E_{SO}(r)$ is calculated by the following Nernst equation [10]:

$$E_{SO}(r) = -\frac{RT_{ELE}(r)}{4F}\ln\frac{p_{ANO\text{-}O_2}(r)}{p_{CATH\text{-}O_2}(r)}. \quad (29)$$

The ohmic voltage drop of the circular planar SOFC ϕ_{SO} is given by:

$$\phi_{SO}(r) = l_{ELE}\rho\exp\left[\frac{a}{T_{ELE}(r)} + b\right]J_{SO}(r), \quad (30)$$

where a and b are constants whose values are estimated to be 6815 and −6.35, respectively, from the I–V characteristics of the circular planar SOFC at 973 and 1073 K [15].

The average current density in the circular planar SOFC $J_{SO\text{-}AVE}$ is given by:

$$J_{SO\text{-}AVE} = \frac{2}{r_0^2}\int_0^{r_0} rJ_{SO}(r)\,dr. \quad (31)$$

The fuel utilization rate in the seal-less planar SOFC stack $U_{SO\text{-}FUEL}$, the oxygen utilization rate in the seal-less planar SOFC stack $U_{SO\text{-}OX}$, and the gross dc output of the seal-less planar SOFC stack $W_{SO\text{-dc}}$ are given by:

$$U_{SO\text{-}FUEL} = 100\frac{\left(M_{SO\text{-}CH_4\text{-}IN} - \frac{N\pi r_0^2 J_{SO\text{-}AVE}}{8F}\right)}{M_{SO\text{-}CH_4\text{-}IN}}, \quad (32)$$

$$U_{SO\text{-}OX} = 100\frac{\left(M_{SO\text{-}O_2\text{-}IN} - \frac{N\pi r_0^2 J_{SO\text{-}AVE}}{4F}\right)}{M_{SO\text{-}O_2\text{-}IN}}, \quad (33)$$

and

$$W_{SO\text{-dc}} = 2\pi N V_{SO}\int_0^{r_0} rJ_{SO}(r)\,dr, \quad (34)$$

where N is the number of SOFC stack units in the stack and r_0 is the radius of the circular planar SOFC. We determined the combustion exhaust heat $Q_{SO\text{-}COM}$ as:

$$Q_{SO\text{-}COM} = \frac{100 - U_{SO\text{-}FUEL}}{100}M_{SO\text{-}CH_4\text{-}IN}\Delta H_{CH_4\text{-}OXI}. \quad (35)$$

The relationship between T_{SO} and J_{AVE} is determined so that the electrical efficiency in the simple SO state, where electricity is generated only in the seal-less planar SOFC stack, $\eta_{SIMP\text{-dc}}$ is 40%. The relationship is summarized in Table 2.

The energy balance in the combustion plenum of the seal-less planar SOFC stack is expressed by:

$$
\begin{aligned}
&-Q_{\text{COM-EXC}} \\
&\quad -\Delta H_{\text{CH}_4\text{-OXI}}(M_{\text{SO-CH}_4\text{-OUT}} + M_{\text{PE-CH}_4\text{-OUT}}) \\
&\quad -\Delta H_{\text{H}_2\text{-OXI}}(M_{\text{SO-H}_2\text{-OUT}} + M_{\text{PE-H}_2\text{-OUT}}) \\
&\quad -\Delta H_{\text{CO}} M_{\text{SO-CO-OUT}} = C_{\text{O}_2} M_{\text{SO-O}_2\text{-OUT}} \\
&\quad \times (T_{\text{COM-OUT}} - T_{\text{SO-AIR-OUT}}) \\
&\quad + C_{\text{N}_2} M_{\text{SO-N}_2\text{-OUT}}(T_{\text{COM-OUT}} - T_{\text{SO-AIR-OUT}}) \\
&\quad + \sum_i C_i M_{\text{SO-}i\text{-OUT}}(T_{\text{COM-OUT}} - T_{\text{SO-FUEL-OUT}}) \\
&\quad + \sum_i C_i M_{\text{PE-}i\text{-OUT}}(T_{\text{COM-OUT}} - T_{\text{PE-FUEL-OUT}}). \qquad (36)
\end{aligned}
$$

4.2. Parallel SOFC–PEFC system

Equilibrium constants of the steam reforming reaction and shift reaction are expressed by:

$$K_{\text{SRR}}(T_{\text{SO-FUEL-OUT}}) = \frac{p^3_{\text{SR-H}_2\text{-OUT}} p_{\text{SR-CO-OUT}}}{p_{\text{SR-CH}_4\text{-OUT}} p_{\text{SR-H}_2\text{O-OUT}}}, \qquad (37)$$

$$K_{\text{SHIF}}(T_{\text{SO-FUEL-OUT}}) = \frac{p_{\text{SR-CO}_2\text{-OUT}} p_{\text{SR-H}_2\text{-OUT}}}{p_{\text{SR-CO-OUT}} p_{\text{SR-H}_2\text{O-OUT}}}, \qquad (38)$$

using the partial pressure of each gas component at the steam reformer outlet. Excess heat of combustion $Q_{\text{COM-EXC}}$ is:

$$
\begin{aligned}
&Q_{\text{COM-EXC}} \\
&\quad = Q_{\text{PE-SR}} - (C_{\text{CH}_4} M_{\text{SR-CH}_4\text{-IN}} + C_{\text{H}_2\text{O}} M_{\text{SR-H}_2\text{O-IN}}) \\
&\qquad \times (T_{\text{SR-IN}} - T_{\text{SR-OUT}}) + Q_{\text{SR-RAD}}, \qquad (39)
\end{aligned}
$$

where the reaction heat used in the steam reformer for PEFC fuel $Q_{\text{PE-SR}}$ is given by:

$$
\begin{aligned}
Q_{\text{PE-SR}} &= \Delta H_{\text{SR}}(M_{\text{SR-CH}_4\text{-IN}} - M_{\text{SR-CH}_4\text{-OUT}}) \\
&\quad + \Delta H_{\text{SHIF}}(M_{\text{SR-CO}_2\text{-OUT}} - M_{\text{SR-CO}_2\text{-IN}}), \qquad (40)
\end{aligned}
$$

and radiation heat from the steam reformer $Q_{\text{SR-RAD}}$ is [16]:

$$Q_{\text{SR-RAD}} = \frac{2\pi N l_{\text{SO}} \lambda_{\text{INS}}(T_{\text{SO}})}{\ln[(r_0 + d + l_{\text{INS}})/(r_0 + d)]}(T_{\text{SO}} - T_{\text{AMB}}). \qquad (41)$$

The thermal conductivity of the ceramic fiber blanket [17] is used for the thermal conductivity of the heat insulator $\lambda_{\text{INS}}(T_{\text{SO}})$.

The molar flow rate of hydrogen in the gas fed to the PEFC stack $M_{\text{PE-H}_2\text{-IN}}$ is given by:

$$M_{\text{PE-H}_2\text{-IN}} = M_{\text{SR-H}_2\text{-OUT}} + 0.99 M_{\text{SR-CO-OUT}}. \qquad (42)$$

The gross dc output of the PEFC stack $W_{\text{PE-dc}}$ is calculated from the fuel utilization rate in the PEFC stack $U_{\text{PE-FUEL}}$, the cell voltage of the PEFC V_{PE}, and $M_{\text{PE-H}_2\text{-IN}}$ using the following equation:

$$W_{\text{PE-dc}} = \frac{2 M_{\text{PE-H}_2\text{-IN}} U_{\text{PE-FUEL}} V_{\text{PE}} F}{100}. \qquad (43)$$

Table 3
Relationship between SOFC operation temperature T_{SO} and heat transfer area of the heat exchangers (HE1–HE3)

T_{SO} (K)	Heat transfer area (m^2)		
	HE1	HE2	HE3
873	0.262	0.468	2.66
923	0.338	0.614	3.43
973	0.429	0.792	4.33
1023	0.544	1.02	5.49
1073	0.674	1.28	6.81

The energy balance in the vaporizer is given by:

$$
\begin{aligned}
&(T_{\text{COM-OUT}} - T_{\text{VAP-OUT}}) C_{\text{CEG}} M_{\text{CEG}} \\
&\quad = [C_{\text{H}_2\text{O}}(T_{\text{VAP}} - T_{\text{AMB}}) + Q_{\text{VAP}}] \\
&\qquad \times (M_{\text{SO-H}_2\text{O-IN}} + M_{\text{SR-H}_2\text{O-IN}}), \qquad (44)
\end{aligned}
$$

where Q_{VAP} is heat of water vaporization ($=4.2 \times 10^4\ \text{J mol}^{-1}$). Temperatures of the methane, steam, and air at the seal-less planar SOFC stack inlet are calculated using the energy balance equation in the heat exchangers and the equation for determining amount of exchanged heat in the heat exchangers [6]. The relationship between T_{SO} and heat transfer area of HE1–HE3 are determined so that $U_{\text{SO-OX}}$ in the simple SO state, where electricity is generated only in the seal-less planar SOFC stack, is equal to 30%. The relationship is summarized in Table 3.

The net ac output of the SOFC stack $W_{\text{SO-ac}}$ and that of the PEFC stack $W_{\text{PE-ac}}$ are given by:

$$W_{\text{SO-ac}} = \zeta(1 - L_{\text{AUX-SO}}) W_{\text{SO-dc}}, \qquad (45)$$

$$W_{\text{PE-ac}} = \zeta(1 - L_{\text{AUX-PE}}) W_{\text{PE-dc}}, \qquad (46)$$

where the ratio of the power consumption in the auxiliary machine to the gross ac output of the seal-less planar SOFC stack $L_{\text{AUX-SO}}$ is calculated by:

$$L_{\text{AUX-SO}} = \frac{30 L_{\text{BLOW}}}{U_{\text{SO-OX}}} + L_{\text{OTHER}}. \qquad (47)$$

The electrical efficiency at the gross dc of the SOFC–PEFC system η_{dc} and that at the net ac of the SOFC–PEFC system η_{ac} are given by:

$$\eta_{\text{dc}} = -\frac{100(W_{\text{PE-dc}} + W_{\text{SO-dc}})}{\Delta H_{\text{CH}_4\text{-OXI}}(M_{\text{SO-CH}_4\text{-IN}} + M_{\text{SR-CH}_4\text{-IN}})}, \qquad (48)$$

$$\eta_{\text{ac}} = -\frac{100(W_{\text{PE-ac}} + W_{\text{SO-ac}})}{\Delta H_{\text{CH}_4\text{-OXI}}(M_{\text{SO-CH}_4\text{-IN}} + M_{\text{SR-CH}_4\text{-IN}})}. \qquad (49)$$

Table 4
Comparison of simulation and experimental results

	$W_{SO\text{-}ac}$ (W)	η_{ac} (%)
Experimental [8]	1029	40
Simulation	1032	40

5. Results and discussion

5.1. Comparison of simulation with experimental results

We compared the simulation result in the simple SO state, where electricity is generated only in the seal-less planar SOFC stack, with the experimental result for a simple SOFC system using a seal-less planar SOFC stack without a depleted fuel plenum [8]. The results are summarized in Table 4. The simulation result agreed with the experimental result, from which we conclude that our simulation can estimate the output and electrical efficiency of the system.

5.2. Influence of heat for PEFC fuel reforming on electrical efficiency

Higher electrical efficiency is expected for the parallel SOFC–PEFC system than for a simple SOFC system using only the seal-less planar SOFC stack since combustion exhaust heat is used for the reforming of the PEFC fuel in the former. Much more combustion exhaust heat is used effectively in the parallel SOFC–PEFC system.

As shown in Fig. 7, the net ac output of the PEFC stack $W_{PE\text{-}ac}$ is proportional to PEFC fuel reforming heat $Q_{PE\text{-}REF}$. This is because the PEFC fuel, which is reformed in the steam reformer and fed to the PEFC stack, increases with increasing $Q_{PE\text{-}REF}$, though the PEFC cell voltage V_{PE}, the ratio of PEFC auxiliary power consumption to the net ac output $L_{AUX\text{-}PE}$, and the PEFC fuel utilization ratio $U_{PE\text{-}FUEL}$ were assumed to be constant. The $W_{PE\text{-}ac}$ and $Q_{PE\text{-}REF}$ are 0 in the simple SO state. $Q_{PE\text{-}REF}$ is increased from the value in the simple SO state (0 W) by decreasing the combustion exhaust heat discharged with air $Q_{EXH\text{-}AIR}$, as expressed in Eq. (15). On the other hand, the net ac output of the SOFC stack $W_{SO\text{-}ac}$ is almost constant as shown in Fig. 7. The gross dc output of the SOFC stack $W_{SO\text{-}dc}$, which is the direct output from the stack, decreases with increasing $Q_{PE\text{-}REF}$, since the molar flow rate of SOFC air $M_{SO\text{-}AIR\text{-}IN}$ is decreased in order to increase $Q_{PE\text{-}REF}$, though the molar flow rate of SOFC methane is kept constant. The electromotive force of the SOFC stack E_{SO} decreases with decreasing $M_{SO\text{-}AIR\text{-}IN}$, since the partial pressure of the oxygen at the cathode side of the circular planar SOFC decreases with decreasing $M_{SO\text{-}AIR\text{-}IN}$. The decrement of E_{SO} causes the decrement of the SOFC cell voltage V_{SO} and that of the gross dc output of the SOFC stack $W_{SO\text{-}dc}$. However, the ratio of the auxiliary power consumption to the net ac output $L_{AUX\text{-}SO}$ decreases with decreasing $M_{SO\text{-}AIR\text{-}IN}$, since the power consumption of the blower for the SOFC air, which is included in the auxiliary power consumption, decreases. Consequently, the net ac output of the SOFC stack $W_{SO\text{-}ac}$ is almost constant. Reforming heat $Q_{PE\text{-}REF}$ is limited to 250 W. This is because the temperature of the exhaust gas T_{EXH} decreases with decreasing exhaust heat $Q_{EXH\text{-}AIR}$ and because T_{EXH} reaches the temperature limit (373 K, assumption V in Section 3.2) when $Q_{PE\text{-}REF}$ is 250 W:

$$Q_{PE\text{-}REF\text{-}MAX} \equiv \max_{M_{SO\text{-}AIR\text{-}IN}} Q_{PE\text{-}REF} = Q_{PE\text{-}REF}|_{T_{EXH}=373\,K}. \quad (50)$$

The electrical efficiency η_{ac} increases with increasing $W_{PE\text{-}ac}$ as shown in Fig. 7. This is because the utilization of the combustion exhaust heat contributes to the electrical efficiency. The maximum η_{ac} is 40%, which is 5% higher than electrical efficiency at the net ac of the parallel SOFC–PEFC system in the simple SO state $\eta_{SIMP\text{-}ac}$. This means that the electrical efficiency in the parallel SOFC–PEFC system is 5% higher than that of the simple SOFC system since the former generates electricity only in the seal-less planar SOFC stack in the simple SO state. When η_{ac} is maximum, the net ac output of the parallel SOFC–PEFC system is 1400 W ($W_{SO\text{-}ac}$, 920 W; $W_{PE\text{-}ac}$, 480 W).

The parallel SOFC–PEFC systems provide higher electrical efficiency than the simple SOFC system, though the exhaust heat utilization mechanism in the parallel SOFC–PEFC system is different from that of the series SOFC–PEFC system using the seal-less tubular SOFC stack with a depleted fuel plenum [6]. However, the increment of η_{ac} is smaller in the parallel SOFC–PEFC system than in the series SOFC–PEFC system. This is because part of combustion exhaust heat has to be used for water vaporization in the parallel SOFC–PEFC system as mentioned in Section 2.

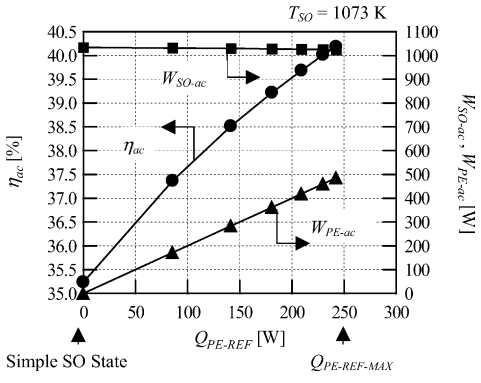

Fig. 7. Influence of the heat used for PEFC fuel reforming $Q_{PE\text{-}REF}$ on net ac output of the SOFC stack $W_{SO\text{-}ac}$, on net ac output of the PEFC stack $W_{PE\text{-}ac}$, and on electrical efficiency at net ac of the parallel SOFC–PEFC system η_{ac} (SOFC operation temperature T_{SO} is 1073 K).

5.3. Influence of SOFC operation temperature on electrical efficiency

In this subsection, the influence of heat $Q_{PE\text{-}REF}$ on $W_{PE\text{-}ac}$ and on electrical efficiency η_{ac} is discussed for various operation temperatures T_{SO} using Figs. 8 and 9.

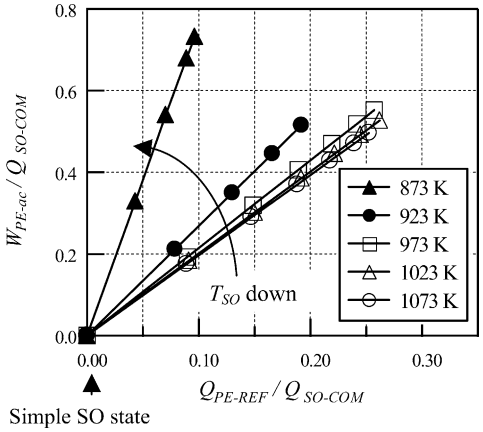

Fig. 8. Influence of the heat used for PEFC fuel reforming $Q_{PE\text{-}REF}$ on net ac output of the PEFC stack $W_{PE\text{-}ac}$ for various SOFC operation temperatures T_{SO} ($Q_{PE\text{-}REF}$ and $W_{PE\text{-}ac}$ are normalized by the combustion exhaust heat of the SOFC fuel $Q_{SO\text{-}COM}$).

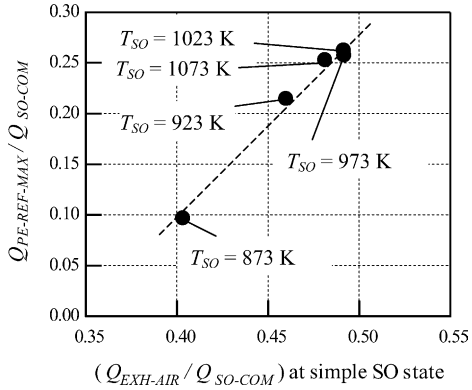

Fig. 10. Relationship between maximum heat used for PEFC fuel reforming $Q_{PE\text{-}REF\text{-}MAX}$ and combustion exhaust heat discharged with air $Q_{EXH\text{-}AIR}$ in the simple SO state ($Q_{PE\text{-}REF\text{-}MAX}$ and $Q_{EXH\text{-}AIR}$ are normalized by the combustion exhaust heat of the SOFC fuel $Q_{SO\text{-}COM}$).

Normalized power $W_{PE\text{-}ac}/Q_{SO\text{-}COM}$ is proportional to normalized heat $Q_{PE\text{-}REF}/Q_{SO\text{-}COM}$ for various T_{SO} as shown in Fig. 8. The normalized power $W_{PE\text{-}ac}/Q_{SO\text{-}COM}$ and heat $Q_{PE\text{-}REF}/Q_{SO\text{-}COM}$ are 0 in the simple SO state. $Q_{PE\text{-}REF}$ is increased from the value in the basic state (0 W) by decreasing the combustion exhaust heat discharged with air $Q_{EXH\text{-}AIR}$ [Eq. (15)]. On the other hand, normalized power $W_{SO\text{-}ac}/Q_{SO\text{-}COM}$ is almost constant (not shown in Fig. 8). Normalized maximum reforming heat $Q_{PE\text{-}REF\text{-}MAX}$ as expressed in Eq. (50) $Q_{PE\text{-}REF\text{-}MAX}/Q_{SO\text{-}COM}$ depends on T_{SO}. The $Q_{PE\text{-}REF\text{-}MAX}/Q_{SO\text{-}COM}$ has a strong relation with the ratio of the exhaust heat $Q_{EXH\text{-}AIR}$ to the combustion heat $Q_{SO\text{-}COM}$ in the simple SO state as shown in Fig. 10. This result agrees with Eq. (15). Note that $Q_{PE\text{-}REF}$ is largest when $Q_{EXH\text{-}AIR}$, which is almost proportional to air flow rate $M_{SO\text{-}AIR\text{-}IN}$, is smallest. The gradient of normalized output $W_{PE\text{-}ac}/Q_{SO\text{-}COM}$ becomes large when T_{SO} decreases as shown in Fig. 8. The reason for this is as follows. The methane conversion rate in the steam reformer decreases with decreasing T_{SO} as shown in Fig. 11. The unreformed methane goes to the combustion plenum in the seal-less planar SOFC stack via the shift converter, CO selective oxidizer, condenser, and PEFC stack. The unreformed PEFC methane is burnt in the combustion plenum. The combustion exhaust heat of the unreformed PEFC methane is also used for the reforming of the PEFC methane. That is, combustion of the unreformed PEFC methane contributes to the increment of $W_{PE\text{-}ac}$. Further, combustion exhaust heat of the unreformed PEFC methane is not included in $Q_{PE\text{-}REF}$ and $Q_{SO\text{-}COM}$. The gradient of normalized output $W_{PE\text{-}ac}/Q_{SO\text{-}COM}$ therefore becomes large when the methane conversion rate decreases with decreasing T_{SO}.

Electrical efficiency η_{ac} is proportional to normalized heat $Q_{PE\text{-}REF}/Q_{SO\text{-}COM}$ for various T_{SO} as shown in Fig. 9. This is because the increment of $Q_{PE\text{-}REF}$ contributes to the η_{ac}. The proportional constants are approximately independent of T_{SO}. As a result, η_{ac} at $Q_{PE\text{-}REF\text{-}MAX}$ for T_{SO} of 873, 923,

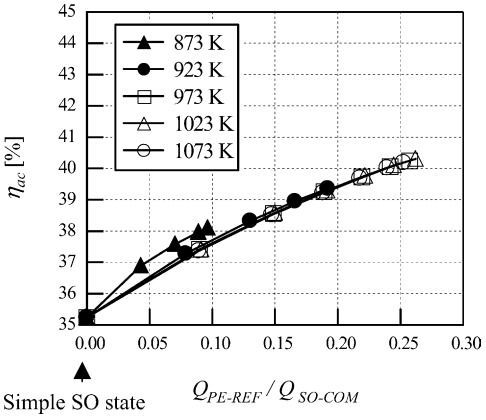

Fig. 9. Influence of the heat used for PEFC fuel reforming $Q_{PE\text{-}REF}$ on electrical efficiency at net ac of the parallel SOFC–PEFC system η_{ac} for various SOFC operation temperatures T_{SO} ($Q_{PE\text{-}REF}$ is normalized by the combustion exhaust heat of the SOFC fuel $Q_{SO\text{-}COM}$).

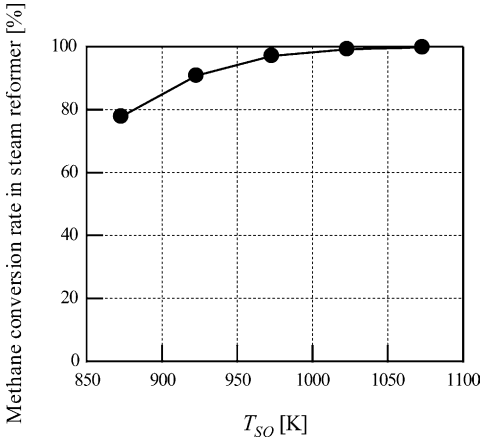

Fig. 11. Influence of the SOFC operation temperature T_{SO} on the methane conversion rate in the steam reformer.

Table 5
Net ac output of the parallel SOFC–PEFC system, net ac output of the seal-less planar SOFC stack $W_{SO\text{-}ac}$, net ac output of the PEFC stack $W_{PE\text{-}ac}$, and electrical efficiency at net ac of the parallel SOFC–PEFC system η_{ac} for various SOFC operation temperatures T_{SO} (These are the values when the heat used for PEFC fuel reforming $Q_{PE\text{-}REF}$ is largest)

T_{SO} (K)	Net ac output of parallel SOFC–PEFC system, $W_{SO\text{-}ac}$, $W_{PE\text{-}ac}$ (W)	η_{ac} (%)
873	800, 440, 360	38
923	940, 580, 360	39
973	1120, 710, 410	40
1023	1280, 820, 460	40
1073	1400, 920, 480	40

973, 1023, and 1073 K are 38, 39, 40, 40, and 40%, respectively. The η_{ac} at $Q_{PE\text{-}REF\text{-}MAX}$ has a strong relationship with normalized heat $Q_{PE\text{-}REF\text{-}MAX}/Q_{SO\text{-}COM}$, which has a correlation with normalized heat $Q_{EXH\text{-}AIR}/Q_{SO\text{-}COM}$ in the simple SO state as shown in Fig. 10. The electrical efficiency in the parallel SOFC–PEFC system is 5% higher than that of the simple SOFC system when T_{SO} is higher than 973 K. The net ac output of the parallel SOFC–PEFC system and η_{ac} at maximum $Q_{PE\text{-}REF}$ for T_{SO} of 873, 923, 973, 1023, and 1073 K are listed in Table 5. $W_{SO\text{-}ac}$ and $W_{PE\text{-}ac}$ at $Q_{PE\text{-}REF\text{-}MAX}$ are also listed in Table 5.

6. Conclusion

We proposed a parallel fuel-feeding SOFC–PEFC system (parallel SOFC–PEFC system) that can use a seal-less planar SOFC stack without a depleted fuel plenum. The steam reformer for the PEFC fuel surrounds the seal-less planar SOFC stack. Combustion exhaust heat from the seal-less planar SOFC stack is used for the reforming of the PEFC fuel. The exhaust heat utilization mechanism in the parallel SOFC–PEFC system is different from that in a series-gas-feeding SOFC–PEFC system (series SOFC–PEFC system) using a seal-less tubular SOFC stack with a depleted fuel plenum. We demonstrated that the parallel SOFC–PEFC system provides higher electrical efficiency than a simple SOFC system that uses the seal-less planar SOFC stack only. The main reason for this is that combustion exhaust heat is used for the reforming of the PEFC fuel in the former. Much more combustion exhaust heat is used effectively in the parallel SOFC–PEFC system than in the simple SOFC system. However, the increment of the electrical efficiency in the parallel SOFC–PEFC system is smaller than that in the series SOFC–PEFC system. This is because part of the combustion exhaust heat has to be used for water vaporization in the parallel SOFC–PEFC system. We evaluated the influence of the SOFC operation temperature on the electrical efficiency and showed the electrical efficiency in the parallel SOFC–PEFC system is 5% higher than that of the simple SOFC system when the SOFC operation temperature is higher than 973 K.

References

[1] J. Larminie, A. Dicks, Fuel Cell Systems Explained, Wiley, 2000, pp. 123–134.
[2] S.E. Veyo, W.L. Lundberg, Proceedings of the International Gas Turbine and Aeroengine Congress and Exhibition, 1999, Paper 99-GT-550.
[3] S.E. Veyo, L.A. Shockling, J.T. Dedere, J.E. Gillett, W.L. Lundberg, Proceedings of the International Gas Turbine and Aeroengine Congress and Exhibition, 2000, Paper 2000-GT-550.
[4] H.E. Vollmar, C.U. Maier, C. Nolscher, T. Merklein, M. Poppinger, J. Power Source 86 (2000) 90–97.
[5] A.L. Dicks, R.G. Fellows, C.M. Mescal, C. Seymour, J. Power Source 86 (2000) 501–506.
[6] M. Yokoo, T. Take, J. Power Source 137 (2004) 206–215.
[7] T. Yamada, N. Chitose, J. Akikusa, N. Murakami, T. Akbay, K. Adachi, A. Hasegawa, K. Hoshino, K. Hosoi, N. Komada, H. Yoshida, T. Sasaki, T. Inagaki, T. Ishihara, Y. Takita, Fuel Cell Seminar Abstracts, 2002, pp. 917–920.
[8] M. Yamada, T. Yamada, N. Chitose, J. Akikusa, N. Murakami, T. Miyazawa, T. Akbay, K. Adachi, T. Kotani, K. Hoshino, K. Hosoi, N. Komada, T. Inagaki, H. Nishiwaki, J. Kanou, H. Nakajima, T. Sasaki, M. Miyata, H. Yoshida, M. Kawano, K. Hashino, Y. Miki, Y. Takita, T. Ishihara, Proceedings of the 12th Symposium on Solid Oxide Fuel Cells in Japan Extended Abstracts, 2003, pp. 20–23 (in Japanese).
[9] L.J.M.J. Blomen, M.N. Mugerwa, Fuel Cell Systems, Plenum Press, 1993, pp. 138–139.
[10] S. Nagata, Y. Kasuga, Y. Ono, Y. Kaga, H. Sato, Trans. Inst. Electr. Eng. Jpn. 107 (B-3) (1982) 147–154 (in Japanese).
[11] L.J.M.J. Blomen, M.N. Mugerwa, Fuel Cell Systems, Plenum Press, 1993, pp. 493–495.
[12] N. Kato, K. Uchimoto, K. Kudo, N. Makita, M. Murai, K. Mine, Proceedings of Intelec 2003, 2003, pp. 77–83.
[13] The Japan Society of Mechanical Engineers, JSME Data Book: Heat transfer, 4th ed., The Japan Society of Mechanical Engineers, 1986, pp. 50–52 (in Japanese).
[14] E. Erdle, J. Groos, H.G. Muller, W.J.C. Muller, R. Sonnenschein, Report of EUR 13158 EN, Commission of the European Communities, 1991.
[15] T. Inagaki, H. Yoshida, T. Sasaki, K. Miura, K. Adachi, K. Hoshino, K. Hosoi, S. Ohara, T. Fukui, T. Ishihara, Fuel Cell Seminar Abstracts, 2002, pp. 423–425.
[16] The Japan Society of Mechanical Engineers, JSME Data Book: Heat transfer, 4th ed., The Japan Society of Mechanical Engineers, 1986, p. 5 (in Japanese).
[17] Japan Society of Thermophysical Properties: Thermophysical Properties Handbook, Yokonedo, 1990, pp. 216–218 (in Japanese).
[18] T. Yatake, A. Sonai, S. Matsuda, A. Kano, Proceedings of Fuel Cell Symposium, 2001, pp. 76–83 (in Japanese).